IOPscience iopscience.iop.org

Home Search Collections Journals About Contact us My IOPscience

Coulomb explosion sputtering of selectively oxidized Si

This article has been downloaded from IOPscience. Please scroll down to see the full text article.

2010 J. Phys.: Condens. Matter 22 175005

(http://iopscience.iop.org/0953-8984/22/17/175005)

View the table of contents for this issue, or go to the journal homepage for more

Download details:
IP Address: 129.252.86.83
The article was downloaded on 30/05/2010 at 07:52

Please note that terms and conditions apply.

J. Phys.: Condens. Matter **22** (2010) 175005 (5pp) doi:10.1088/0953-8984/22/17/175005

Coulomb explosion sputtering of selectively oxidized Si

P Karmakar[1,3], S Bhattacharjee[2], V Naik[1], A K Sinha[2] and A Chakrabarti[1]

[1] RIB Laboratory, Variable Energy Cyclotron Centre, 1/AF, Bidhannagar, Kolkata 700 064, India
[2] UGC-DAE CSR, Kolkata Centre, III/LB-8, Bidhannagar, Kolkata 700 098, India

E-mail: prasantak@veccal.ernet.in

Received 19 January 2010, in final form 24 February 2010
Published 7 April 2010
Online at stacks.iop.org/JPhysCM/22/175005

Abstract
We have studied the sputtering of a unique system comprising of coexisting silicon and silicon oxide surfaces due to the impact of multiply charged Ar^{q+} ions. Such surfaces are produced by oblique angle oxygen ion bombardment on Si(100), which results in one side oxidized ripple formation due to preferential oxygen implantation. It is observed by atomic force microscopy and conducting atomic force microscopy studies that the higher the potential energy of the Ar^{q+} ion, the higher the sputtering yield of the nonconducting (oxide) side of the ripple as compared to the semiconducting side while ensuring an identical irradiation and measurement condition. It also shows experimentally the potential of highly charged ions in the gentle cleaning or tailoring of nanostructures. The results are explained in terms of the Coulomb explosion model, where potential sputtering depends on the conductivity of the ion impact sites.

(Some figures in this article are in colour only in the electronic version)

1. Introduction

Low energy (∼keV) single and multicharged ion beam induced nanostructure formation has been studied intensively in recent years. Singly charged energetic ions transfer their kinetic energy to the target atoms and create surface nanostructures following a sputtering and diffusion mechanism [1, 2]. In contrast, multicharge ions (MCI) carry an internal (i.e. potential) energy corresponding to the sum of the binding energies of the removed q electrons, in addition to the kinetic energy. During the interaction with the solid surface the MCI regains its missing q electrons to become neutralized, resulting in hollow atom formation, electron emission, photon emission and potential sputtering [3, 4].

The investigation of potential sputtering is one of the most active research areas because such an erosion mechanism is fundamentally interesting as well as important for potential applications in defect less cleaning, material selective etching and as gentle tool for nanostructuring [5]. A number of investigations have been reported for different materials such as Au(111), HOPG, CaF_2(111), LiF(001), TiO_2(110), Si(111), SiO_2 [6], and ultrathin Pt film [7]. Such investigations are carried out with a range of tools, which include direct sputtering yield measurement by mass loss estimation, secondary ion emission measurement, secondary electron counting, and topographical measurement by scanning probe microscopy. Each of these techniques has its own individual limitations, whether due to thermal fluctuation, charge accumulation, counting statistics, or contamination or matrix effect. Very recently, the erosion of thin oxide layers of magnetic tunnel junctions by 361 keV Xe^{44+} has been estimated by measuring the change of conductance of the thin layer [8]. However, the high kinetic energy of the highly charged ions (HCI), and the subsequent metal electrode deposition on the HCI irradiated ultrathin oxide layer for conductance measurement, might modify the system, which makes it difficult to accurately extract the contribution of potential energy on sputtering. Nevertheless, the models of potential sputtering dictate that the interaction of MCI depends highly on the conductivity of the target surface [5]. Therefore, it is of great interest to carry out studies pinpointing the effect of the potential energy of MCI on a surface having different conductive sectors in the nanometer scale.

In this work, a novel technique has been employed to study the fundamentals of potential sputtering and the effectiveness

[3] Author to whom any correspondence should be addressed.

 © 2010 IOP Publishing Ltd Printed in the UK & the USA

of such sputtering in gentle tailoring of nanostructures. Spatially resolved semiconducting and insulating surfaces of nano-ripples are bombarded with multicharged Ar^{q+} ions. The initial nano-ripple structures are formed by oblique angle single charged oxygen ion bombardment on Si(100), where one side of each ripple is semiconducting and the other side is poorly conducting due to preferential oxygen implantation. The dependence of potential sputtering on surface conductivity is shown by comparing the sputtering erosion of coexisting semiconducting and poorly conducting surfaces (which ensures the identical conditions for irradiation and measurement) by topographic and conductivity imaging before and after MCI impact.

2. Experimental details

Si(100) samples were cleaned with trichloroethylene and then methanol in an ultrasonic bath. The cleaned and dried Si(100) samples were then transferred to a target chamber for oblique angle oxygen ion irradiation. The samples were first irradiated with a 16 keV O_2^+ ion beam at 60° angle with respect to the surface normal at a fluence of 2×10^{18} atoms cm^{-2}. The topography and surface conductivity measurements were carried out in air by scanning probe microscopy (Nanoscope IV, Digital Instrument), in contact atomic force microscopy (AFM) and conducting atomic force microscopy (C-AFM) modes. The samples were again placed in the irradiation chamber and bombarded with $^{40}Ar^{q+}$ ($q = 2$, 3, 8, 9) ions at normal incidence for symmetric bombardment of both the oxidized and non-oxidized part of the ripple structures. The kinetic energy of the Ar^{q+} ions was the same (32 keV) in all cases. The MCI irradiation was also carried out at grazing incidence (70°) where a strong kinetic component of the ion beam is parallel to the ripple direction and only a weak component is along normal direction. All the ions were generated and extracted from the 6.4 GHz ECR ion source of the radioactive ion beam facility at the Variable Energy Cyclotron Centre Kolkata [9]. After Ar^{q+} bombardment, the nanostructures are again imaged by the AFM and C-AFM in air. For C-AFM measurements the bias between the tip and sample was 4 V.

3. Results and discussion

The ripple formation and selective oxidation are both evident from figure 1. It is well established [1] that nanoscale ripple structures are formed during the oblique angle ion bombardment on Si(100). Due to the stochastic nature of the incident ions, random roughness is generated on the initial flat surface, leading to the development of local curvature. [10]. For subsequent ion bombardment at oblique angle, ripple structures are formed on Si(100) because of the competition between the curvature dependent sputtering and surface diffusion induced flattening. [1, 2]. Once the structures are formed, the effective ion impact angle with respect to the local surface normal differs from the ion incidence angle (60°), thus, the local ion impact angle on the beam facing surface of the ripple is reduced, whereas for the other side of the ripple it is increased (figure 1). This results in an increase of implanted

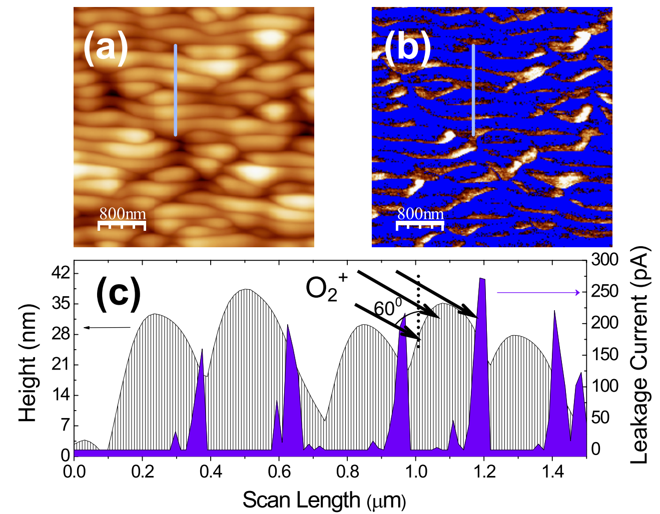

Figure 1. Same area (a) AFM and (b) C-AFM images of Si ripple structures produced by 16 keV O_2^+ bombardment at 60°. (c) Superposition of one-dimensional topographic and current profiles corresponding to the marked lines. The arrow indicates the O_2^+ beam direction.

oxygen concentration, leading to oxidation in the beam facing side of the ripple (figure 1). This compositional change causes a further reduction of the sputtering yield from the beam facing surface, and thus the surface of each ripple is decomposed into two phases: a more oxidized portion facing the ion beam and a less oxidized portion on the other side of the ripple. Figure 1(a) presents the topographic AFM image and figure 1(b) shows the C-AFM current image of the same area, from measurements of the leakage current through the sample for a fixed bias voltage between the tip and the sample. For better comparison, the line profiles of the topographic and current images are superimposed in figure 1(c). Figure 1(c) shows clearly that the leakage current is substantial only at the back side of the ripple, which confirms the coexistence of insulating and semiconducting sectors of the nano-ripples. Homma *et al* reported similar structures for 2–10 keV O_2^+ bombardment at 45°, and Auger mapping showed the asymmetric distribution of implanted oxygen [11]. C-AFM measurement at the bottom of the SIMS crater formed by 8 keV O_2^+ ions also reveals the same fact [12]. Preferential incorporation of projectile ions in the beam facing slope of the ripple is also reported in the cases of 60 keV Ar^+ bombarded Si ripples and 16.7 keV O_2^+ bombarded Al ripples at an incidence angle of 60° [13, 14]. Such ripples offer an interesting system where both semiconducting and insulating surfaces coexist. Here, we have exploited such a system to study the role of surface conductivity on the MCI induced potential sputtering.

C-AFM measurement of the ripple structures after impact of Ar^{q+} revealed that the oxide area of the ripples is eroded more than the semiconducting part with an increase of the charge state of the projectile, though the kinetic energies were the same. Figure 2 shows representative AFM and C-AFM images after Ar^{3+} and Ar^{8+} bombardment. Figure 2(a1) illustrates the topography of Ar^{3+} bombarded Si ripples and figure 2(a2) shows the conducting zones of the corresponding ripples. Figure 2(a3) represents the superposition of the line

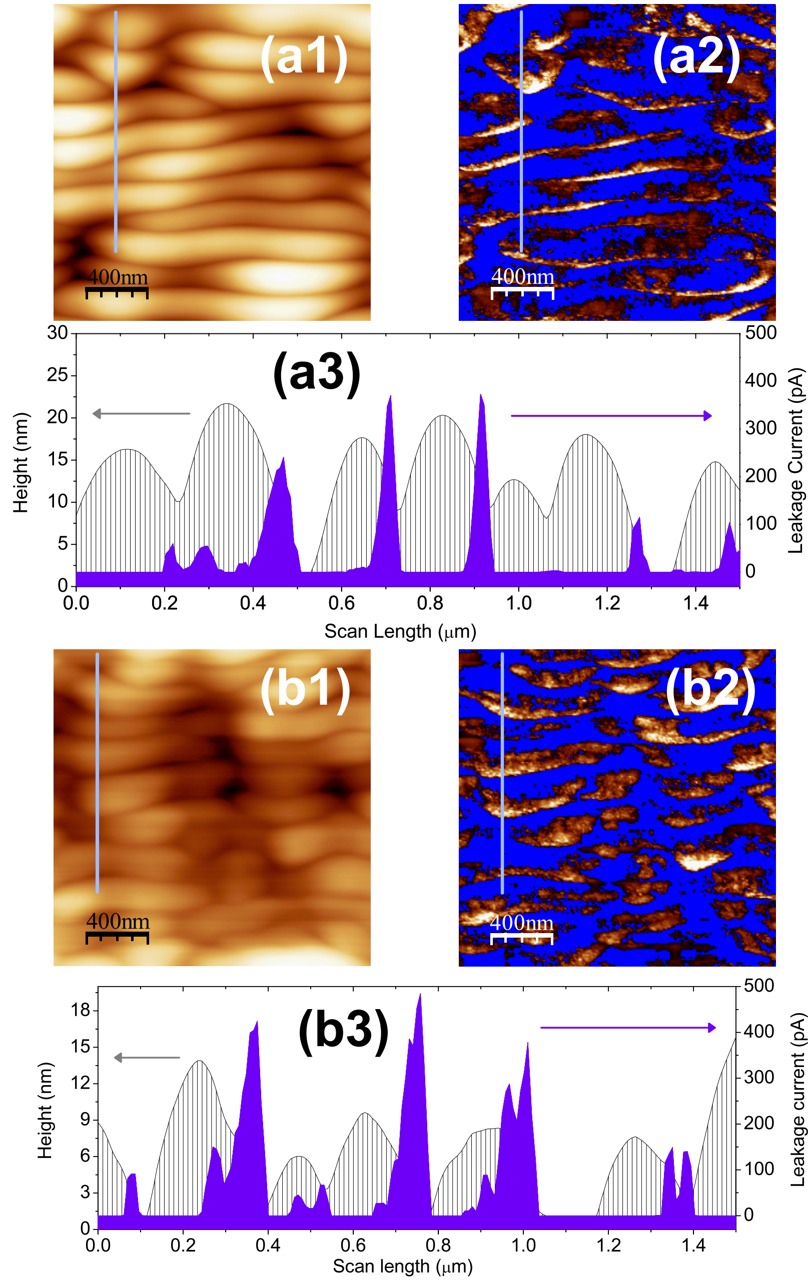

Figure 2. (a) After 32 keV Ar^{3+} bombardment at a fluence 2×10^{16} ions cm^{-2}; (a1) AFM topography of the ripple structures; (a2) C-AFM image of the same area showing only the conducting zones; (a3) superposition of topographic (black stripe) and current (filled) profiles, corresponding to the marked lines. (b) After 32 keV Ar^{8+} bombardment at fluence 2×10^{16} ions cm^{-2}; (b1) AFM topography of the ripple structures; (b2) C-AFM image of the same area showing only the conducting zones; (b3) superposition of topographic (black stripe) and current (filled) profiles, corresponding to the marked lines.

profiles along the marked lines on the topographic and current images. Similarly, figures 2(b1), (b2) and (b3) show the AFM, C-AFM and superposition of line profiles, respectively, of Ar^{8+} bombarded rippled structures. It is clear from figures 2(a1) to (b3) that in the case of Ar^{8+} bombardment the area of the conducting zones of the ripples are increased compared to Ar^{3+} bombardment, although kinetic energies are the same in both the cases. In the present experiment the MCI ions carry both kinetic and potential energy, as they are not decelerated. Therefore, the total sputtering yield (Y_{total}) due to the impact of MCI could be expressed as $Y_{total} = Y_{ke} + Y_{ps}$ where Y_{ke} is due to kinetic sputtering and Y_{ps} is due to potential sputtering. To investigate the effect of potential energy, the same kinetic energy ($V \times q = 32$ keV) of the Ar^{q+} ($q = 2, 3, 8, 9$) ions was maintained, where V is the extraction voltage and q is the charge state of the ions. Therefore, the erosion of ripples due to kinetic energy (32 keV) of the Ar^{3+} and Ar^{8+} cases is expected to be similar. In the case of Ar^{3+} the stored potential energy is only 84 eV and thus almost equal erosion of both sides of the ripple is expected due to the dominant kinetic sputtering, however, the increase of conducting area (figure 2), i.e., the preferential erosion of the oxide part of the ripple after

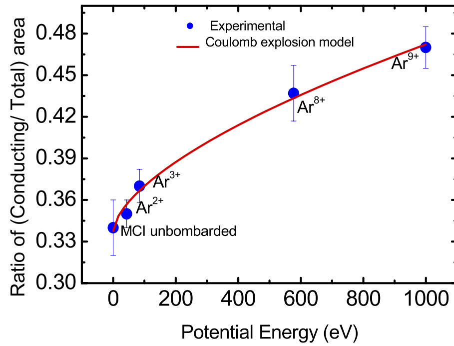

Figure 3. Ratio of conducting (Si) area to total area as a function of projectile (Ar^{q+}) potential energy.

Ar^{8+} bombardment reveals the effect of the potential energy (577 eV) stored in the incident ions.

A large number of C-AFM and AFM images were taken on the Ar^{q+} ($q = 2, 3, 8, 9$) bombarded ripple structures and analyzed with the software WSxM [15]. The total projected area of the ripple structures is obtained by projecting the three-dimensional (x, y, z) AFM data on a two-dimensional (x, y) plane. Similarly the projected area of the conducting part is acquired from C-AFM data (figure 2). The ratio of the conducting and total areas of the ripple structures is calculated from each pair of C-AFM and AFM images. The average values of the ratio are plotted as a function of the projectile potential energy, shown in figure 3. It is observed that the ratio 'conducting/total' increases with projectile potential energy, which means the higher the potential energy, the higher the erosion of the oxide part of the ripples as compared to the non-oxide part.

The potential sputtering due to impact of MCI has been explained by different existing models [16]. In defect induced desorption model [17], it is assumed that holes and electron hole pairs are created in the valance band of the target following the neutralization and relaxation of the MCI. In the case of alkali halides, the coupling to the lattice is strong, leading to trapping of the holes and electron–hole pairs. This leads to the formation of self-trapped holes and self-trapped excitons. These defects decay further into color centers which may diffuse to the surface and lead to desorption of the target atoms. But the defect induced desorption model is shown to be effective only for crystals where a strong electron–phonon coupling is present, e.g. the alkali halides, some oxides and oxidized surfaces.

An inelastic thermal spike model, originally developed for swift heavy ion (SHI) induced hillock formation, has been applied for hillock formation on the MCI irradiated CaF_2 by El-Said *et al* [18]. During SHI ion bombardment the material in the ion track is rapidly heated by the electronic energy loss process. If the local temperature exceeds the melting point, the lattice melts and hillocks are created due to relaxation of the internal stress produced by SHI. Although similar local melting and hillock formation is found by MCI impact, excitation of the lattice due to the neutralization of MCI is fundamentally different from the excitation mechanism by SHI. This model works well for heavy and very high charge state ion surface interaction.

A number of experimental observations [7, 19] have been successfully explained by the Coulomb explosion model proposed by Parillis [20]. In this model, when the MCI comes close to the target surface, the electrons from the surface fill the high lying Rydberg states of the projectile. The emission of electrons from the surface forms charge depletion at the impact point. If the surface is a good conductor, the conduction electrons quickly diminish the charged up domain prior to the explosion, but for a poor conductor this charge imbalance will survive for a sufficient duration because of the limited diffusion length of the electron. Therefore, the situation can be described by the relation between the two timescales τ_i and τ_e, where τ_i is the effective time of Auger processes causing the creation of positively charged domain around the multiply charged projectile and τ_e is the time of neutralization of this domain by conducting electrons. For a poor conductor $\tau_i \ll \tau_e$.

The charge domain formed under MCI impact is assumed to be a hemisphere of radius R_0. The potential energy 'W' is shared between the Coulomb repulsion energy (E_c) and the kinetic energy of the Auger electrons [7, 20]. The 'W' could be written as $W \sim R_0^5$ from the energy balance equation [20]. The potential sputtering yield is given by $Y_{ps} = 0.49\pi n(R_0 - a)^3$, [7, 20] where n is the number of charged atoms in a unit volume and a is the thickness of the layer from which no particle would succeed to escape during the neutralization time τ_e. Therefore, the potential sputtering yield Y_{ps} is proportional to $W^{3/5}$ in the Coulomb explosion model.

The present observation has been compared with the Coulomb explosion model by plotting the ratio of Si to total (Si and SiO_2) areas with the projectile potential energy, as shown in figure 3. The change in the ratio of 'conducting/total area' with potential energy gives a measure of enhanced sputtering of the oxide part of the ripple. A fit (solid line) to the experimental data shows a $W^{0.62\pm0.09}$ dependence, which is in good agreement with the Coulomb explosion model. Tona *et al* [19] studied the secondary ion emission during the impact of I^{q+} on a native SiO_2 thin film on Si(111) (an insulator surface) and a clean well defined hydrogen terminated Si(111) (semiconductor) surface. The authors also reported the potential sputtering of an ultrathin Pt film in terms of the Coulomb explosion model. But in the present case, the direct comparison of the sputtering yield of coexisting insulating and semiconducting regions of the nano-ripples reduces the difficulties of maintaining the identical experimental conditions and also allows one to estimate the total sputtering by nanometer scale measurement.

Although the kinetic energy of the projectiles was kept constant in all cases, it is better to study the potential effect by reducing the kinetic energy of the projectiles. To reduce the kinetic component along the surface normal, we bombarded with the same ion beam (32 keV Ar^{q+}) at grazing (70°) incidence and along the ripple orientation. The observation shows no difference in sputtering between the oxide and non-oxide part of the ripples for Ar^{2+} and Ar^{8+} bombardment (data not shown). Peng *et al* [21] recently reported sputtering of SiO_2 by Ar^{q+}/Pb^{q+} and showed that at larger incidence angles, the sputtering yield is dominated by elastic collision between the incident ion and material atoms. They also reported that

the smaller the incident angle, the larger the contribution from the potential sputtering. Therefore, the present observation is consistent with Peng *et al* [21]. However, preferential sputtering of the nonconducting part would be stronger if a projectile with higher potential and lower kinetic energy at normal incidence is used.

4. Conclusion

The present experiment clearly establishes one of the fundamentals of MCI–surface interaction, i.e., the dependence of potential energy erosion on the conductivity of the ion impact site by comparing the sputtering of coexisting oxide and non-oxide surfaces under identical conditions. It shows the capability of multicharge ions in selective etching of the surface on the nanometer scale and opens up an exciting way to tailor the shape and dimension of nanostructures by ion beam.

Acknowledgments

The authors thank the members of the RIB group who helped during the ECR operation. The authors would also like to thank Professor D Ghose for access to the SPM and Mr S A Mollick for assistance during the SPM measurement.

References

[1] Chan W L and Chason E 2007 *J. Appl. Phys.* **101** 121301
[2] Muñoz-García J, Vázquez L, Cuerno R, Sánchez-García J A, Castro M and Gago R 2007 arXiv:0706.2625v1 [cond-mat.mtrl-sci]
[3] Gillaspy J D 2001 *J. Phys. B: At. Mol. Opt. Phys.* **34** R93
[4] Karmakar P, Agarwal P, Nabhiraj P Y, Bose D K, Bhandari R K and Ghose D 2001 *Phys. Rev.* A **64** 034901
[5] Aumayr F and Winter H 2003 *e-J Surf. Sci. Nanotechnol.* **1** 171
[6] Aumayr F, El-Said A S and Meissl W 2008 *Nucl. Instrum. Methods Phys. Res.* B **266** 2729
[7] Ghose D, Karmakar P and Parilis E 2003 *Nucl. Instrum. Methods Phys. Res.* B **212** 420
[8] Pomeroy J M and Grube H 2009 *Nucl. Instrum. Methods* B **267** 642
[9] Chakrabarti A 2007 *Nucl. Instrum. Methods* B **261** 1018
[10] Karmakar P, Mollick S A, Ghose D and Chakrabarti A 2008 *Appl. Phys. Lett.* **93** 103102
[11] Homma Y, Takano A and Higashi Y 2003 *Appl. Surf. Sci.* **203/204** 35
[12] Gautier B, Fares B, Prudon G and Dupuy J-C 2004 *Appl. Surf. Sci.* **231/232** 136
[13] Datta D P and Chini T K 2005 *Phys. Rev.* B **71** 235308
[14] Mishra P, Karmakar P and Ghose D 2006 *Nucl. Instrum. Methods* B **243** 16
[15] Horcas I, Fernandez R, Gomez-Rodriguez J M, Colchero J, Gomez-Herrero J and Baro A M 2007 *Rev. Sci. Instrum.* **78** 013705
[16] Facsko S, Heller R, El-Said A S, Meissl W and Aumayr F 2009 *J. Phys.: Condens. Matter* **21** 224012
[17] Neidhart T, Pichler F, Aumayr F, Winter H P, Schmid M and Verga P 1995 *Phys. Rev. Lett.* **74** 5280
[18] El-Said A S, Heller R, Meissl W, Ritter R, Facsko S, Lemell C, Solleder B, Gebeshuber I C, Betz G, Toulemonde M, Moller W, Burgdorfer J and Aumayr F 2008 *Phys. Rev. Lett.* **100** 237601
[19] Tona M, Takahashi S, Nagata K, Yoshiyasu N, Yamada C, Nakamura N, Ohtani S and Sakurai M 2005 *Appl. Phys. Lett.* **87** 224102
[20] Parillis E 2001 *Trapping Highly Charged Ions: Fundamentals and Applications* ed J Gillaspy (Huntington, NY: Nova Science) chapter 17, p 407
[21] Peng H B, Cheng R, Yang X Y, Han Y C, Zhao Y T, Yang J, Wang S W, Fang Y and Wang T S 2009 *Surf. Coat. Technol.* **203** 2387